

Multicolor Graphene Nanoribbon/Semiconductor Nanowire Heterojunction Light-Emitting Diodes

*Yu Ye,^a Lin Gan,^b Lun Dai,^{*a} Hu Meng,^a Feng Wei,^a Yu Dai,^a Zujin Shi,^b Bin Yu,^a
Xuefeng Guo,^b and Guogang Qin^{*a}*

a State Key Lab for Mesoscopic Physics and School of Physics, Peking University,
Beijing 100871, China

b College of Chemistry and Molecular Engineering, Peking University, Beijing
100871, China

* To whom correspondence should be addressed. E-mail: lundai@pku.edu.cn (L. D.);
qingg@pku.edu.cn (G. Q.).

Supporting Information

The electrical properties of the graphene nanoribbon (GNR)

The electrical properties of the GNRs fabricated with the method used in this work were investigated by measuring their transistor characteristics. The GNR transistor was fabricated by using an insulative SiO₂ NW as the mask. In this case, the NW mask needs not to be removed before the measurement, and thus eliminates some unnecessary process induced influence to the measured results. Figure S1a-c illustrates our approach of fabricating a GNR transistor. First, the as-synthesized large-scale graphene was transferred by the stamp method with the help of PMMA on a *p*⁺-Si/600 nm SiO₂ substrate. Then, the insulating SiO₂ nanowires (NWs) dispersed in ethanol were dropped on the substrate (Figure S1a). Second, the ohmic contact source and drain electrodes (60 nm Au) for the graphene were defined at the two terminals of a NW using UV lithography followed by thermal evaporation and lift-off process (Figure S1b). Finally, oxygen plasma etching (ICP-98A) was used to remove the exposed graphene with the Au electrodes and the SiO₂ NW as the masks (Figure S1c). In this GNR transistor, the *p*⁺-Si substrate was used as the back gate, and the 600 nm SiO₂ was used as the gate dielectric. Figure S1d shows an FESEM image of a fabricated GNR transistor. The room-temperature source-drain current (I_{DS}) vs source-drain voltage (V_{DS}) relations at various back-gate voltages (V_G) are shown in Figure S1d. During the measurement, the source was grounded. We can see clearly that the conductance decreases as V_G increases toward a positive direction (Figure S1e), demonstrating that the GNR is *p*-type. The gate transfer curve measured at $V_{DS}=0.1$ V is shown in Fig. S1f. The charge neutral point is located at $V_G \sim 37$ V. The transconductance $g_m = \partial I_{DS} / \partial V_G$ (calculated from the linear region of the I_{DS} - V_G curve at V_G near to zero) is ~ 6.15 nA/V. The carrier mobility can be calculated

from $\mu = \frac{hg_m}{\epsilon\epsilon_0} \frac{L}{WV_{DS}}$,^{S1, S2} where h (~ 600 nm) and ϵ (=3.9) are the thickness and relative dielectric constant of gate dielectric, respectively, L (~ 5.4 μ m) and W are the length and width of GNR, respectively. ϵ_0 is vacuum permittivity. In order to measure the GNR width, we removed the SiO_2 NW by an ultrasonic process. From the FESEM image shown in the inset of Figure S1d, we obtained the GNR width to be ~ 190 nm, a bit narrower than the SiO_2 NW atop (~ 215 nm), confirming the formation of an undercut during the oxygen plasma etching process. The hole mobility is thus estimated to be ~ 303 $\text{cm}^2/\text{V}\cdot\text{s}$ at V_G near to zero, which is about three times higher than that obtained from Hall-effect measurement (98.6 $\text{cm}^2/\text{V}\cdot\text{s}$). It has long been noticed that the carrier mobility is usually higher in semiconductor NWs than in their film or bulk counterparts. One possible explanation for this is that the quasi 1D nature of NWs may play a significant role in terms of reducing the low-angle carrier scattering.^{S3} The reason for the mobility increase in GNR in our case is still under study.

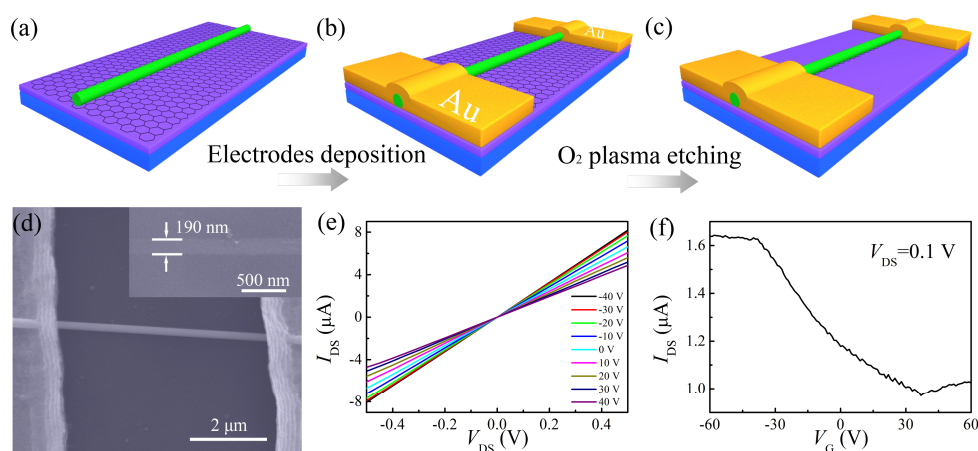


Figure S1. (a)-(c). Schematic illustration of the fabrication processes of the GNR transistor. (d). FESEM image of the measured GNR transistor. Inset: the FESEM image of the GNR in the transistor. (e). Room-temperature I_{DS} - V_{DS} characteristics of the GNR transistor at various V_G . V_G changes from -40 to 40 V in a step of 10 V. (f).

The gate transfer characteristics of the GNR transistor at $V_{DS}=0.1$ V.

In order to estimate the contact resistance of GNR used in our devices, we employed the four-terminal measurement method. Figure S2a shows an FESEM image of a fabricated device for four-terminal measurement. The device fabrication processes are similar as those described in the manuscript except that herein four Au (60 nm) ohmic contact electrodes were defined across an insulative SiO_2 nanowire (NW) on a graphene. The Au (60 nm) electrodes and the SiO_2 NW also served as the masks for later-on oxygen plasma etching. During the measurement, a current source was applied to the outer two electrodes, while the voltage was read out from the inner two electrodes. In this case, we can obtain the resistance of the GNR between the two inner electrodes to be about 25.0 k Ω . The measured result is shown in Figure S2b. For comparison, the two terminal $I-V$ result measured between the two inner electrodes is also plotted in the figure, which gives a resistance (including the GNB resistance and the two contact resistances) to be about 30.8 k Ω . Thus, the total contact resistance between the two electrodes and the GNR can be estimate to be about 5.8 k Ω .

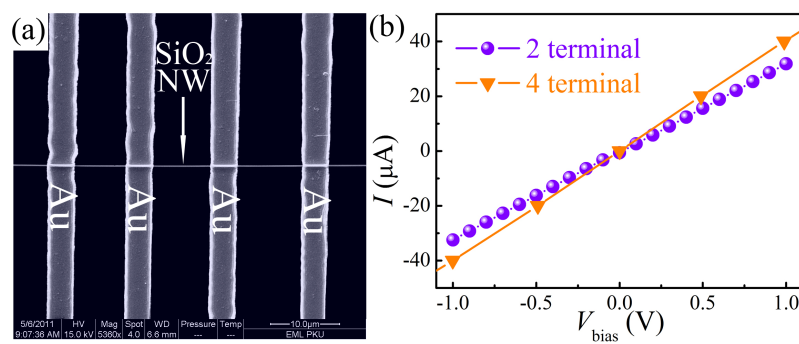


Figure S2. (a) An FESEM image of a fabricated device for four-terminal measurement.
(b) The $I-V$ curves obtained from the two-terminal and the four-terminal measurements.

HRTEM, Raman and transparency measurements of the as-synthesized graphene

Figure S3a shows the transparency spectrum of the graphene, which was measured by a UV-vis-NIR recording spectrophotometer (Shimadzu UV-3100). It can be seen that high transparency (> 98%) occurs in the range of wavelength longer than 500 nm. Figure S3b shows a typical HRTEM image of the graphenes. The fringe at the edge provides evidence that the graphene is monolayer. Electron diffraction on the graphene (the inset) reveals a hexagonal pattern, confirming the three-fold symmetry of the carbon atom arrangement, and indicating the high crystalline of the graphene. Figure S3c shows a typical Raman spectrum of the graphenes. It shows two main peaks: a narrow linewidth ($\sim 28 \text{ cm}^{-1}$) G-band peak ($\sim 1593 \text{ cm}^{-1}$) and a narrow linewidth ($\sim 50 \text{ cm}^{-1}$) 2D-band peak ($\sim 2692 \text{ cm}^{-1}$). Their intensity ratio ($I_{2\text{D}} : I_G$) is about 2.4, indicating again the formation of monolayer graphene.^{S4} Besides, the defect-related D-band peak ($\sim 1358 \text{ cm}^{-1}$)^{S5} is weak, indicating again the high quality of the graphene.

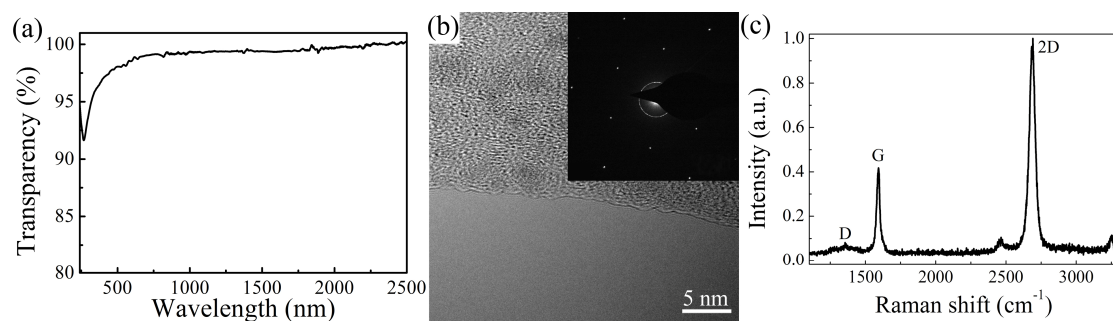


Figure S3 (a) The transparency spectrum of the graphene on a quartz substrate. (b) Typical HRTEM image of an as-synthesized graphene, indicating the formation of monolayer graphene. Inset: selected area electron diffraction (SAED) pattern of the graphene. (c) Raman Spectrum of an as-synthesized graphene on a Si/300 nm SiO₂

substrate.

Electrical transport properties of the GNR/ZnO NW and GNR/CdSe NW heterojunction LEDs

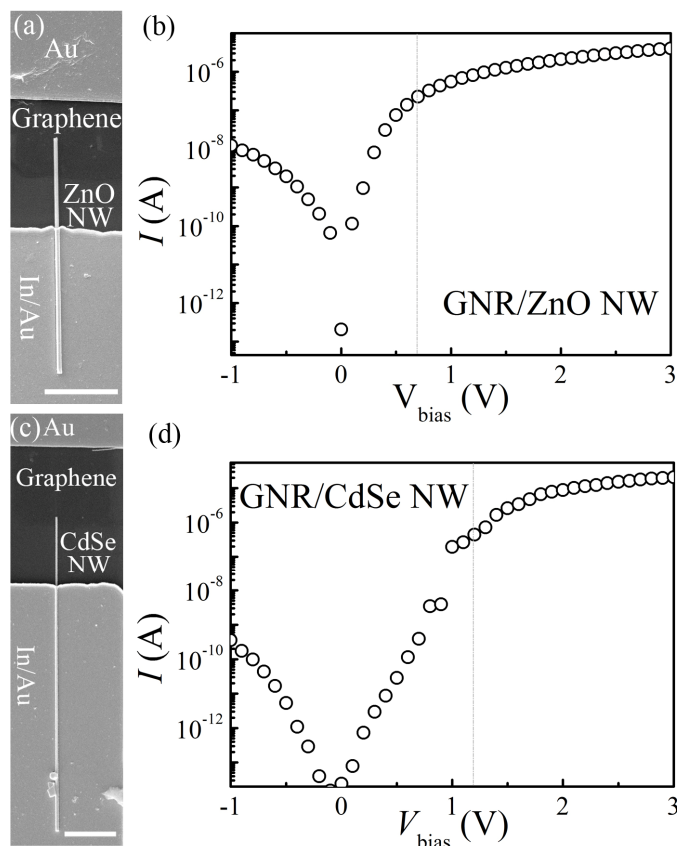


Figure S3. (a) FESEM image of the measured GNR/ZnO NW heterojunction LED. The diameter of the ZnO NW is about 420 nm. Scale bar: 5 μ m. (b) Room-temperature I - V characteristic of the LED in panel (a) on a semilogarithmic scale. (c) FESEM image of the measured GNR/CdSe NW heterojunction LED. The diameter of the CdSe NW is about 300 nm. Scale bar: 5 μ m. (d) Room-temperature I - V characteristic of the LED in panel (c) on a semilogarithmic scale.

From the above figures, we can obtain the turn-on voltages of GNR/ZnO NW and GNR/CdSe NW heterojunctions to be about 0.7 and 1.2 V, respectively.

Graphene pad/SNW and GNR/SNW heterojunction LEDs

For comparison, we also fabricated the LED device, where the GNR was totally removed, and the big graphene pad and In/Au were source and drain contacts of the SNW. The typical *I-V* curve of a graphene pad/*n*-CdS NW heterojunction is shown in Figure S4a, together with that of the GNR/*n*-CdS NW heterojunction depicted in the paper. Herein, the *n*-CdS NWs used were with the same doping level ($\sim 10^{17} \text{ cm}^{-3}$). We can see that the turn-on voltages for the graphene pad/*n*-CdS NW and GNR/*n*-CdS NW heterojunctions are around 1.4 and 1.1 V, respectively. Besides, under identical forward bias, the current for the GNR/SNW heterojunction is higher, indicating the existence of more injected electrons and holes. As a result, light emission can be detected from the GNR/SNW heterojunction at a forward bias as low as 2.5 V, whereas no light emission can be detected from the graphene pad/*n*-CdS NW heterojunction at a forward bias up to 5 V. Figure 2b show the room-temperature EL spectra of the graphene pad/*n*-CdS NW and GNR/*n*-CdS NW heterojunctions at a forward bias of 7 and 4 V, respectively. Similar phenomenon had also been observed before for the Si/SNW heterojunctions.⁵⁶ We think that, compared to the graphene pad/SNW heterojunction, the face-to-face contact structure of GNR/SNW heterojunction has the advantage of larger active region (where the radiative recombination occurs) and smaller series resistance, which may benefit high-efficiency EL, and even electrically driven laser in the future.

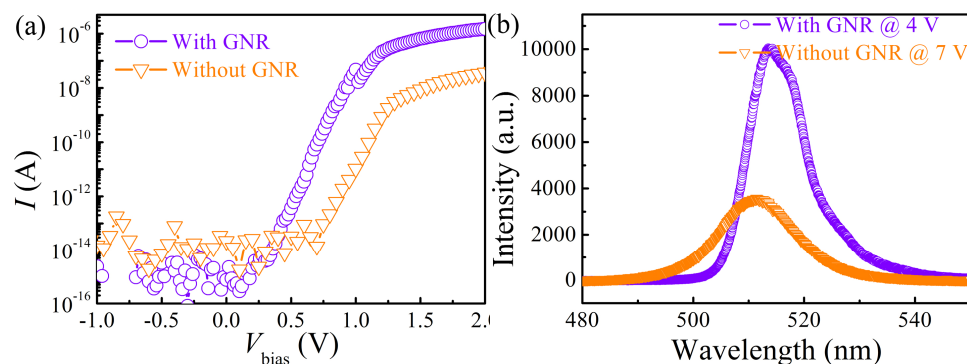


Figure S4. (a) Typical I - V curves of graphene pad/ n -CdS NW and GNR/ n -CdS NW heterojunctions. (b) Room-temperature EL spectra of the graphene pad/ n -CdS NW and GNR/ n -CdS NW heterojunctions at a forward bias of 7 and 4 V, respectively.

References

- (S1) Z. M. Liao, B. H. Han, Y. B. Zhou, D. P. Yu, *J. Chem. Phys.*, 2010, **133**, 044703.
- (S2) N. E. Staley, C. P. Puls, Y. Liu, *Phys. Rev. B*, 2008, **77**, 155429.
- (S3) S. Ju, A. Facchetti, Y. Xuan, J. Liu, F. Ishikawa, P. D. Ye, C. W. Zhou, T. J. Marks, D. B. Janes, *Nature Nanotech.*, 2007, **2**, 378-384.
- (S4) A. Reina, X. T. Jia, J. Ho, D. Nezich, H. Son, V. Bulovic, M. S. Dresselhaus, J. Kong, *Nano Lett.*, 2009, **9**, 30-35.
- (S5) A. C. Ferrari, *Solid State Commun.*, 2007, **143**, 47-57.
- (S6) C. Liu, L. Dai, Y. Ye, T. Sun, R. M. Peng, X. N. Wen, P. C. Wu, G. G. Qin, *J. Mater. Chem.*, 2010, **20**, 5011-5015.